Proceedings of the Thirty-sixth (2026) International Ocean and Polar Engineering Conference
Orlando, Florida, USA, May 31-June 5, 2026

ISBN 978-1-880653-72-2; ISSN 1098-6189
www.isope.org

Investigation of a Wake Model for Floating Offshore Wind Turbines with Vertical Wake Deflection under Pitch Motion

*Mingqiu Liu, Weiwen Zhao, Decheng Wan**

Computational Marine Hydrodynamics Lab (CMHL), School of Ocean and Civil Engineering,
Shanghai Jiao Tong University, Shanghai, China
*Corresponding Author

ABSTRACT

This study employs large eddy simulation (LES) to investigate the effects of platform pitch offset and pitch motion of a floating offshore wind turbine (FOWT) on wake characteristics, and an analytical wake model is developed accordingly. The results indicate that a platform pitch offset induces a systematic upward shift of the wake centerline in the vertical direction, and a more pronounced vertical wake deflection is observed with increasing offset angle. The velocity deficit profiles exhibit an approximately double-peaked feature in the near wake and gradually transition to a single-peaked Gaussian-like distribution with downstream distance; in the far wake, good agreement with a Gaussian distribution is achieved. Based on momentum conservation and a two-dimensional Gaussian velocity distribution assumption, a vertical component of the rotor-induced force associated with an effective inclination angle is incorporated, and an expression for vertical wake deflection is derived. A wind-shear correction is further introduced, leading to an analytical wake model applicable to FOWTs. Validation against LES results demonstrates that the proposed model captures the vertical wake deflection induced by the platform pitch offset and provides accurate predictions of far-wake velocity deficit profiles, offering useful guidance for floating wind farm applications.

KEY WORDS: Large eddy simulation; Actuator line model; FOWT; Analytical wake model; Wake deflection.

INTRODUCTION

In recent years, offshore wind energy has experienced rapid development worldwide. To exploit abundant wind resources in far offshore regions, increasing attention has been directed toward floating offshore wind turbine (FOWT) technology (Bhattacharya and Nikitas, 2025). Under complex marine environmental conditions, FOWTs undergo six-degree-of-freedom (6-DOF) motions, which further influence their aerodynamic performance and wake characteristics. Wake characteristics play a crucial role in determining overall wind farm efficiency and operational safety (Wang et al., 2024). Therefore, the development of wake modeling for FOWTs is essential for wind farm design and performance assessment.

At present, studies on FOWT wakes mainly rely on wind tunnel experiments, numerical simulations, and analytical wake models. Fan and Liu (2025) investigated the wake characteristics of an FOWT under coupled surge and pitch motions at different inflow turbulence intensities using wind tunnel experiments, and reported that coupled motions enhanced mesoscale energy and promoted lateral wake expansion. Messmer et al. (2025) conducted wind tunnel experiments to examine the wake characteristics of an FOWT under surge and sway motions, and showed that large-scale coherent structures accelerated wake recovery through mechanisms such as enhanced Reynolds stress gradients. Wind tunnel experiments can provide highly reliable data; however, their high cost and limited data volume restrict their applicability. In contrast, numerical simulation approaches, particularly computational fluid dynamics (CFD) methods, can provide comprehensive flow field information and are widely adopted in FOWT wake studies.

Cai et al. (2024) investigated the aerodynamic characteristics of an FOWT under combined surge and pitch motions using CFD, in which the wind turbine was modeled with fully resolved blade geometry. The results indicated that large motion amplitudes could trigger dynamic stall and lead to pronounced load fluctuations. Although fully resolved blade-geometry modeling enables detailed resolution of near-blade flow structures, simultaneously resolving blade-scale flow features and far wake regions substantially increases mesh size and computational cost. The actuator line model (ALM) represents wind turbine blades using distributed actuator points, where aerodynamic forces are imposed on the flow field as body forces, significantly reducing computational expense. As a result, ALM is more commonly employed in FOWT wake modeling. Xu et al. (2023) investigated FOWT wake characteristics under atmospheric boundary layer (ABL) inflow conditions using ALM, and reported that platform pitch induced vertical wake center deflection. Li et al. (2024) studied the wake characteristics of an FOWT under surge motion for different inflow conditions and found that surge-induced periodic coherent structures could accelerate wake recovery. Liu et al. (2025) examined the effects of coupled surge-pitch motions on FOWT wake characteristics under ABL inflow conditions. Dynamic mode decomposition showed that dominant wake modes are primarily governed by inflow turbulence, while motion-induced modes exhibit relatively low energy, although low-frequency motions are more effective in exciting pronounced responses. Although CFD methods can provide high-fidelity flow field data, their computational cost remains prohibitive for engineering applications such as wind farm layout optimization and power production assessment. In such cases, analytical wake models are more suitable, as they provide very high computational efficiency while maintaining an acceptable level of accuracy for engineering applications.

Most existing analytical wake models have been developed for fixed-bottom wind turbines (FBWTs), including the widely used Jensen model (Jensen, 1983), the Gaussian wake model (Bastankhah and Porté-Agel, 2014), and various extensions based on these formulations (Wang et al., 2024). However, the 6-DOF motions of FOWTs alter wake structures and velocity distributions, indicating the necessity of developing analytical wake models specifically tailored for FOWTs. Zhang et al. (2024a) proposed an analytical wake model for FOWTs by introducing corrections related to platform position and yaw conditions. Zhang et al. (2024b) developed an analytical wake model for FOWTs under pitch motion, in which the influence of pitch motion on the inflow velocity was considered. Li et al. (2025) proposed a dynamic analytical wake model applicable to FOWTs under surge, heave, and pitch motions.

Despite these efforts, the influence of platform pitch offset on vertical wake deflection has received relatively limited attention in existing analytical wake models. Therefore, the effects of pitch motion on FOWT wake characteristics under ABL inflow conditions are investigated using LES in the present study. Based on the LES results, an analytical wake model is proposed to account for vertical wake deflection induced by the platform pitch offset. The proposed model is validated against LES simulations, and the results demonstrate that it can reasonably predict both the vertical wake center deflection and the associated velocity deficit induced by the platform pitch offset.

NUMERICAL SIMULATION

Large Eddy Simulation

The turbulence modeling approach adopted in the present study is large eddy simulation (LES). LES is widely used in wind turbine wake simulations because unsteady flow features can be captured with good fidelity. The fundamental idea of LES is to separate large-scale and small-scale turbulent motions through spatial filtering. The large-scale motions are resolved directly, whereas the effects of the unresolved small-scale motions are represented using a subgrid-scale model. The filtered incompressible continuity and momentum equations are written as follows:

$$\frac{\partial \bar{u}_i}{\partial x_i} = 0 \tag{1}$$

$$\frac{\partial \bar{u}_i}{\partial t} + \frac{\partial (\bar{u}_i \bar{u}_j)}{\partial x_j} = -\frac{\partial \hat{p}}{\partial x_i} - \frac{\partial \tau_{ij}^D}{\partial x_j} - \frac{1}{\rho_0}\frac{\partial p_0(x,y)}{\partial x_i} + \frac{1}{\rho_0} F_i - \varepsilon_{ijk} f \, \bar{u}_k \tag{2}$$

where, the overbar indicates the spatially resolved quantities; t is time; u is the wind velocity; ρ_0 represents the reference air density; τ_{ij}^D is the deviatoric component of the wind stress tensor; F_i is the force exerted by the wind turbine; g is the gravitational acceleration; ε_{ijk} is the alternating unit tensor; f is the Coriolis parameter; and $\hat{p}$ is the modified pressure. The stress τ_{ij}^D is computed based on the Smagorinsky subgrid-scale model (Smagorinsky, 1963), with the Smagorinsky constant set to 0.13.

Actuator Line Model

The actuator line model (ALM) is an actuator-type approach that is widely employed in wind turbine simulations (Sørensen and Shen, 2002). The basic concept of ALM is to discretize wind turbine blades into a series of actuator points, where the aerodynamic forces at each actuator point are calculated using blade element theory. The aerodynamic forces acting on the actuator points are then distributed to the flow field in the form of body forces, thereby representing the interaction between the wind turbine and the surrounding flow. The volumetric force applied at each actuator point is expressed as follows:

$$f = (L, D) = \frac{1}{2}\rho U_{rel}^2 c\,dr (C_L \vec{e}_L + C_D \vec{e}_D) \tag{3}$$

where, L and D are the lift and drag forces, respectively; U_{rel} is the relative wind speed; c is the chord length; dr is the width of the blade element; C_L and C_D are the lift and drag coefficients, respectively; $\vec{e}_L$ and $\vec{e}_D$ are the unit vectors of lift and drag, respectively.

To simulate FOWTs, an additional velocity component induced by platform motion is incorporated into the calculation of the relative wind speed. Fig. 1 illustrates the velocity vectors acting on the blade element. Here, U_M represents the additional velocity induced by platform motion; U is the inflow wind speed, and the subscripts θ and Z denote the tangential and axial components, respectively. The local attack angle α is defined as:

$$\alpha = \phi - \gamma, \phi = \tan^{-1}\left(\frac{U_Z + U_{M,Z}}{\Omega r + U_{M,\theta} - U_\theta}\right) \tag{4}$$

where, ϕ is the local inflow angle; γ is the local pitch angle, Ω is the rotor speed. After the local attack angle is obtained, the lift and drag coefficients are interpolated from the design airfoil data. To avoid numerical singularities when applying wind turbine body forces to the flow field, a smoothing treatment is required. The Gaussian kernel function is employed to distribute the volumetric forces, thereby ensuring numerical stability of the simulations.

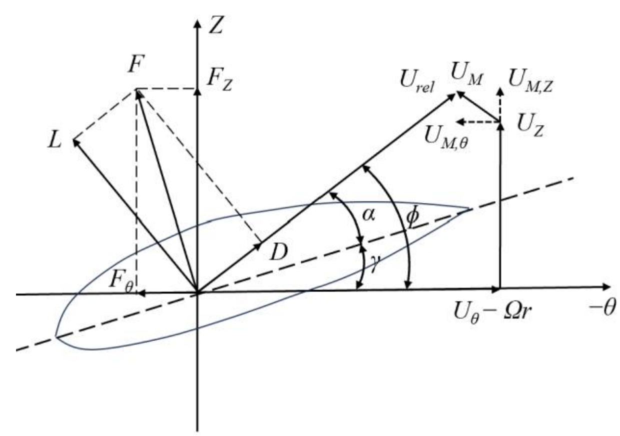

Fig. 1. Velocity vectors acting on the blade element

Numerical Setup

An open-source solver, SOWFA (Simulator for Wind Farm Applications), developed by the National Renewable Energy Laboratory (NREL) based on OpenFOAM, is employed in the present study. SOWFA is capable of simulating FBWTs and can be coupled with FAST to simulate FOWTs (Churchfield et al., 2012). In this work, a prescribed 6-DOF forced-motion module is implemented on top of the original SOWFA framework to represent FOWT motions. The solver has been well validated in previous studies (Churchfield et al., 2012; Liu et al., 2025). The wind turbine is modeled using the NREL 5MW reference turbine (Jonkman et al., 2009), with a rotor diameter of 126 m and a hub height of 90 m. The rated wind speed is 11.4 m/s, and the rated rotor speed is 12.1 rpm. The operating conditions considered in this study are set to the rated state.

The numerical simulations are conducted in two stages: a precursor simulation and a wind turbine simulation. In the precursor stage, an ABL inflow is generated using the precursor approach. The computational domain is a rectangular box of 3000 m × 1000 m × 1000 m, as shown in Fig. 2. A uniform grid spacing of 10 m is applied in all three directions. Cyclic boundary conditions are imposed in the horizontal directions, a slip boundary condition is specified at the top boundary, and the Moeng wall (Moeng, 1984) boundary condition is applied at the bottom boundary. The inflow wind is aligned with the positive x-direction, and the wind speed at hub height is 11.4 m/s. To obtain a quasi-equilibrium ABL, the precursor simulation is run for 18,000 s with a time step of 0.2 s. An additional 1,000 s simulation is then performed to provide inflow data for the wind turbine simulation stage. In the generated ABL, the power-law wind shear exponent is 0.105, and the streamwise turbulence intensity at hub height is 6.02%.

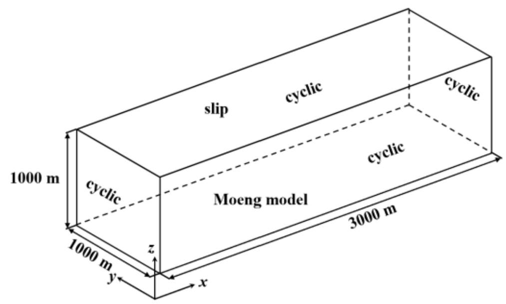

Fig. 2. The computational domain

In the wind turbine simulation stage, the coupled interaction between the FOWT and the ABL flow is modeled. The computational domain and the initial mesh are the same as those adopted in the precursor simulation. The inlet boundary condition is time-dependent and imposed through a mapping method using flow fields extracted from the precursor results, whereas a zero pressure-gradient condition is specified at the outlet. As shown by the black short line in Fig. 3, the wind turbine is placed 6*D* downstream of the inlet (where *D* denotes the rotor diameter). Two refinement levels are introduced within a rectangular region around the turbine. The first refinement zone extends 13*D*, 4*D*, and 2.5*D* in the x, y, and z directions, respectively, with its upstream boundary located 2.5D ahead of the turbine. The second refinement zone covers 12*D*, 3*D*, and 2*D* in the x, y, and z directions, respectively, and begins 2*D* upstream of the turbine. Within the refined region, the grid spacing is 2.5 m × 2.5 m × 2.5 m, yielding approximately 13 million cells in total. The simulation is performed for 1000 s using a time step of 0.02 s to satisfy the CFL requirement. For the verification of mesh and time-step convergence, one can refer to Liu et al. (2025). Since the wake experiences an initial transient before a statistically steady state is established, the first 400 s are excluded from the analysis, and the remaining 600 s of quasi-stationary data are used for subsequent post-processing.

On this basis, prescribed platform pitch motions are applied in the coupled simulations to quantify pitch-induced variations in wake characteristics, particularly the vertical wake deflection. Under combined wind-wave loading, the platform pitch motion generally oscillates about a mean equilibrium position. This mean position is referred to as the platform pitch offset. Accordingly, a sinusoidal pitch oscillation about a prescribed pitch offset is imposed in the present simulations. A schematic illustration of the prescribed pitch motion is shown in Fig. 4. The pitch motion is defined as a rotation about the y-axis, centered at a point located 90 m below the wind turbine hub. The pitch angle and angular velocity are defined as follows:

$$\theta(t) = A_p \sin(2\pi f_p t) + \theta_p \quad (5)$$

$$\omega(t) = 2\pi f_p A_p \cos(2\pi f_p t) \quad (6)$$

where, A_p denotes the pitch motion amplitude; θ_p represents the platform pitch offset, and f_p is the pitch motion frequency. The simulation cases are summarized in Table 1. Case 1 represents FBWT.

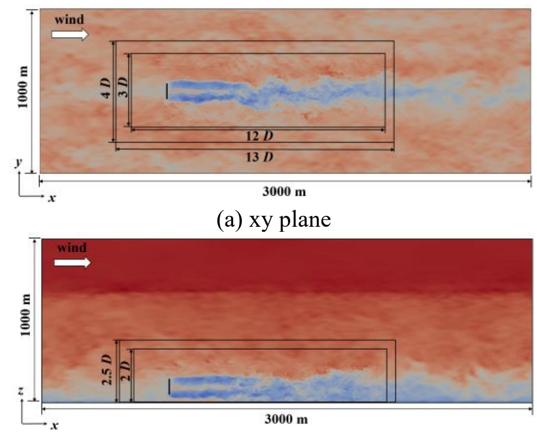

(a) xy plane

(b) xz plane

Fig. 3. Schematic of the computational domain and mesh refinement zone

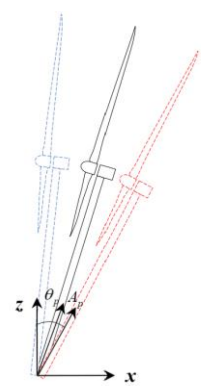

Fig. 4. Schematic of the prescribed pitch motion

Table 1. Case settings

Case	A_p (°)	f_p (Hz)	θ_p (°)
1	-	-	-
2	4	0.1	5
3	4	0.1	10

NUMERICAL RESULTS

Atmospheric Boundary Layer Inflow

The ABL flow field generated in the precursor simulation stage is more representative of realistic atmospheric conditions. Fig. 5 presents the time-averaged profiles of wind speed, wind direction, and streamwise turbulence intensity along the vertical direction. The wind speed profile is normalized by the inflow wind speed at hub height, U_0 = 11.4 m/s. Good agreement is observed between the simulated profile and the theoretical power-law wind shear, with a shear exponent of approximately 0.105. Owing to the Coriolis force, the wind direction varies with height, and a wind-direction difference of about 1.5° is observed between the lowest and highest blade-tip elevations. The streamwise turbulence intensity decreases with height, reaching 6.02% at hub height.

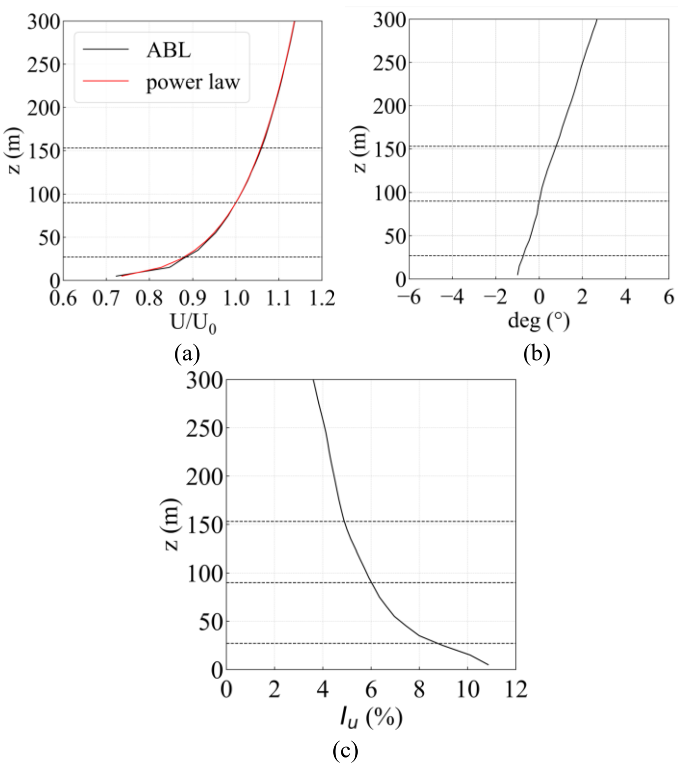

Fig. 5. Time-averaged vertical profiles: (a) normalized wind speed; (b) wind direction; (c) streamwise turbulence intensity

Wake Characteristics

To ensure statistical convergence of the numerical results, the final 600 s of the simulations are selected for post-processing; all subsequent time-averaged quantities are computed over this 600 s time window. Fig. 6 shows the time-averaged streamwise velocity distribution on the horizontal plane at hub height, and Fig. 7 presents the time-averaged streamwise velocity distribution on the vertical plane through the rotor center. The results indicate that, on the horizontal plane, the wake velocity distributions of the FBWT and FOWTs are overall comparable, whereas wake recovery is faster downstream of the FOWTs. In contrast, the vertical plane more clearly reveals that the wake undergoes an overall upward shift as θ_p increases. This indicates that the primary effect of platform pitch offset is not a substantial change in the wake width on the horizontal plane, but a systematic displacement of the wake in the vertical direction.

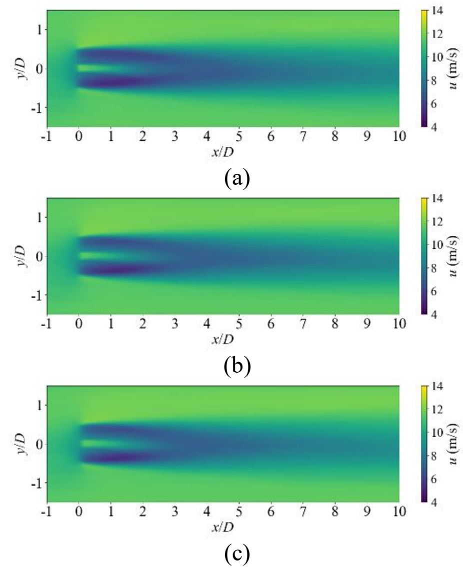

Fig. 6. Time-averaged streamwise velocity field on the horizontal plane at hub height: (a) Case1; (b) Case2; (c) Case3

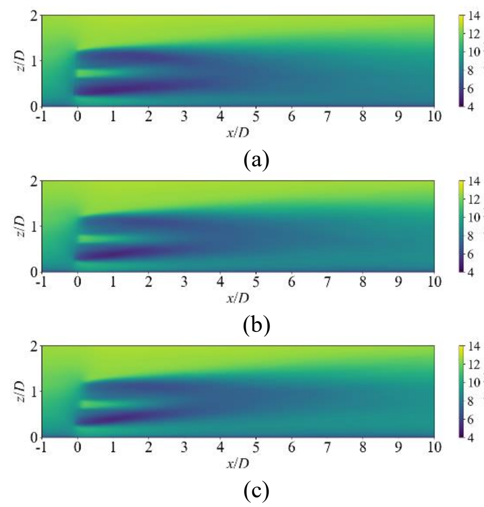

Fig. 7. Time-averaged streamwise velocity field on the vertical plane through the rotor center: (a) Case1; (b) Case2; (c) Case3

Fig. 8 further presents the instantaneous streamwise velocity distribution on the vertical plane through the rotor center (shown at the end of the simulation). A similar upward deflection is also observed in the instantaneous wake of the FOWTs. In addition, coherent structures induced by the pitch motion are visible near the shear layer, and this feature is more pronounced in the near-wake region. Fig. 9 shows the normalized velocity deficit profiles on the horizontal plane at hub height and on the vertical plane through the rotor center. The normalized velocity deficit is defined as $(u_{hub} - u)/u_{hub}$, where u_{hub} is set to 11.4 m/s. As shown in the figure, the velocity deficit distribution in the near wake exhibits an approximately double-peaked Gaussian shape; with increasing downstream distance, the distribution gradually transitions to a single-peaked standard Gaussian shape. This behavior can be attributed to the fact that the near wake is still strongly affected by the rotor-induced velocity deficit, while turbulent mixing gradually smooths these local features as the wake develops downstream. Comparisons among different cases indicate faster wake recovery for the FOWTs. Meanwhile, in the vertical plane, the overall upward wake shift leads to a corresponding change in the location of the maximum velocity deficit.

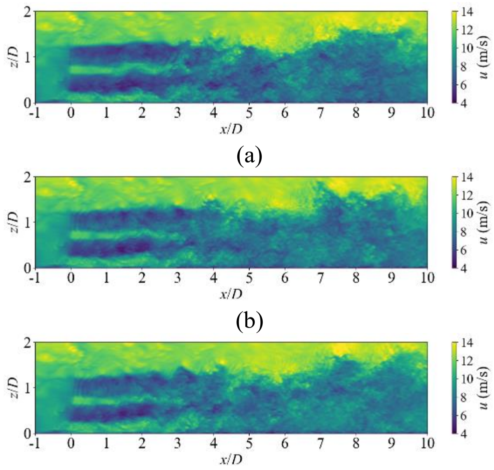

Fig. 8. Instantaneous streamwise velocity field on the vertical plane through the rotor center: (a) Case1; (b) Case2; (c) Case3

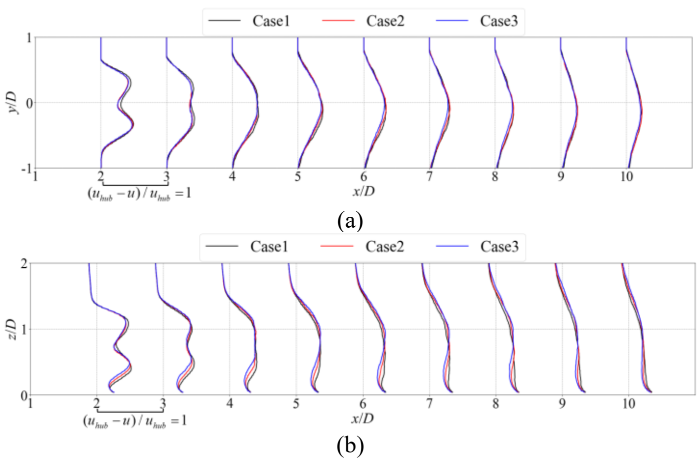

Fig. 9. Normalized velocity deficit profiles: (a) horizontal plane; (b) vertical plane

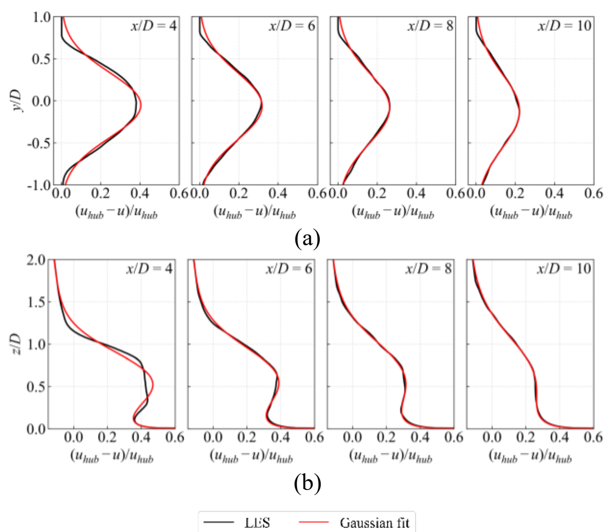

Fig. 10. Comparison between LES results and Gaussian fitting for Case3: (a) horizontal plane; (b) vertical plane

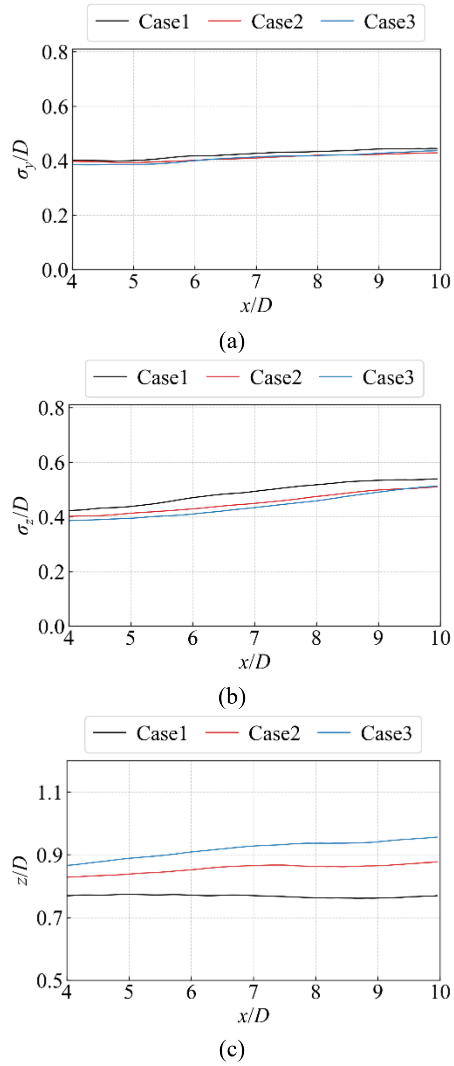

Fig. 11. Gaussian fitting results: (a) Gaussian standard deviation on the horizontal plane; (b) Gaussian standard deviation on the vertical plane; (c) vertical wake centerline position

Fig. 10 compares the LES results of Case 3 with the corresponding Gaussian fitting. Good agreement with a Gaussian distribution is observed in the far wake, and the fitting performance becomes more evident beyond 4*D*. Fig. 11 further presents the Gaussian standard deviations and the vertical wake centerline position obtained from the far-wake Gaussian fitting. The horizontal and vertical standard deviations differ, while the values for the FBWT and FOWTs remain close. In addition, a clear vertical wake deflection is observed with increasing θ_p, and the vertical wake centerline exhibits a pronounced upward shift. These results provide a basis for the development of the subsequent analytical wake model.

A NEW ANALYTICAL WAKE MODEL

Model Derivation

An analytical wake model applicable to FOWTs is proposed in this study, where the vertical wake deflection induced by the platform pitch offset is taken into account. The model development follows the general modeling framework of classical yaw wake models (Bastankhah and Porté-Agel, 2016; Wei et al., 2021; He et al., 2023). Specifically, the Gaussian wake representation and skew-angle formulation are adopted based on Bastankhah and Porté-Agel (2016), while the wake-width formulation and the shear-inflow correction are introduced following He et al. (2023). A schematic of the wind turbine wake is provided in Fig. 12. The derivation is first established under the assumption of uniform inflow conditions to obtain the baseline formulation. The influence of atmospheric shear inflow is then incorporated using the treatment of He et al. (2023). Due to the presence of a platform pitch offset, an effective inclination angle exists between the rotor plane and the incoming flow direction. It is further noted that the wind turbine has a fixed tilt angle θ_t. Therefore, the effective inclination angle is expressed as the sum of the tilt angle and the platform pitch offset, i.e., $\varphi = \theta_p + \theta_t$. Under this inclined condition, the rotor-induced force contains a vertical component, which leads to vertical wake deflection. The region enclosed by the blue line denotes the control volume. The thrust coefficient C_T is defined as follows:

$$C_T = \frac{F}{0.5\rho A_0 \left(u_0 \cos\varphi\right)^2} \tag{7}$$

where, ρ is the air density; A_0 represents the area of rotor; u_0 is the inflow wind speed at the hub height. The rotor-induced force F can be expressed by:

$$F = \frac{1}{2}\rho C_T A_0 \left(u_0 \cos\varphi\right)^2 \tag{8}$$

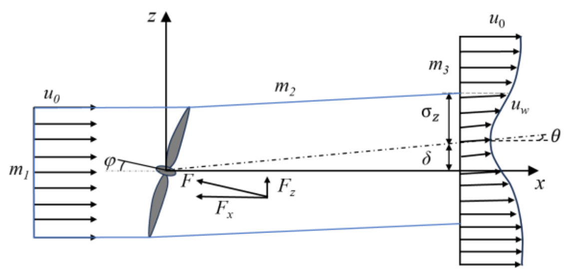

Fig. 12. Schematic of the wind turbine wake

In Fig. 12, m_1 and m_2 denote the mass flow entering the control volume from the rotor plane and the lateral wake boundary, respectively. θ represents the skew angle of the wake velocity. m_3 denotes the mass flow rate leaving the control volume, which is expressed as follows:

$$m_3 = \rho \int_{A_w} u_w \,\mathrm{dA} \tag{9}$$

where, u_w is the wake velocity; A_w represents the area of the wake outlet. According to the conservation of momentum, the streamwise and vertical forces can be expressed by:

$$F_x = \rho \int_{A_w} u_w^2 \cos\theta \,\mathrm{dA} - \left(m_1 + m_2\right) u_0 \tag{10}$$

$$F_z = -\rho \int_{A_w} u_w^2 \sin\theta \,\mathrm{dA} \tag{11}$$

Assuming that θ in the far wake region is close to zero, it can be obtained that $\cos\theta \approx 1$. The following expression can be obtained:

$$\frac{1}{2}\rho C_T A_0 u_0^2 \cos^3\varphi \approx -\rho \int_{A_w} u_w \Delta u \,\mathrm{dA} \tag{12}$$

where, $\Delta u = u_0 - u_w$ denotes the velocity deficit. The wake velocity distribution is assumed to follow a two-dimensional Gaussian profile (Bastankhah and Porté-Agel, 2016; He et al., 2021), which is expressed as follows:

$$u_w = u_0 - \frac{A}{2\pi\sigma_y\sigma_z} e^{-\left(\frac{y^2}{2\sigma_y^2} + \frac{(z-h_0-\delta_z)^2}{2\sigma_z^2}\right)} \tag{13}$$

where, σ_y and σ_z denote standard deviation in horizontal direction and vertical direction, respectively; h_0 is the hub height; δ_z denotes the vertical wake deflection. Following He et al. (2021), the wake half-widths in the two transverse directions are taken as 2.81 times the corresponding standard deviations, i.e., $r_y = 2.81\sigma_y$ and $r_z = 2.81\sigma_z$. The formula for calculating the standard deviation is as follows:

$$\frac{\sigma_y}{D} = k_y \frac{x}{D} + \varepsilon_y \tag{14}$$

$$\frac{\sigma_z}{D} = k_z \frac{x}{D} + \varepsilon_z \tag{15}$$

$$k_y = 0.065 C_T^{0.2566} I_0^{0.2808}, k_z = 0.0866 C_T^{0.4279} I_0^{0.4707} \tag{16}$$

$$\varepsilon_y = 0.2406 C_T^{0.1147} I_0^{0.0124}, \varepsilon_z = 0.2788 C_T^{0.0295} I_0^{0.032} \tag{17}$$

where, I_0 is the streamwise turbulence intensity at hub height. By substituting Eq. (13) into Eq. (12), the following expression is obtained:

$$A = 2\pi\sigma_y\sigma_z u_0 \left(1 - \sqrt{1 - \frac{C_T^{'} D^2}{8\sigma_y\sigma_z}}\right), C_T^{'} = C_T \cos^3\varphi \tag{18}$$

$$u_w = u_0 - u_0 \left(1 - \sqrt{1 - \frac{C_T^{'} D^2}{8\sigma_y\sigma_z}}\right) e^{-\left(\frac{y^2}{2\sigma_y^2} + \frac{(z-h_0-\delta_z)^2}{2\sigma_z^2}\right)} \tag{19}$$

The wake velocity distribution derived above is obtained under the assumption of a uniform inflow. Following He et al. (2021), a momentum correction accounting for shear inflow is introduced. The resulting velocity deficit distribution is expressed as follows:

$$u_w = u_0 \left(\frac{z}{z_0}\right)^{\alpha} - u_0 \left(1 - \sqrt{1 - \frac{C_T^{'} D^2}{8\sigma_y\sigma_z}}\right) e^{-\left(\frac{y^2}{2\sigma_y^2} + \frac{(z-h_0-\delta_z)^2}{2\sigma_z^2}\right)} - \frac{2a \iint_{Sr1} \Delta u \,\mathrm{d}A}{\pi r_y r_z} \tag{20}$$

$$a = \frac{1 - \sqrt{1 - C_T^{'}}}{2} \tag{21}$$

$$r_1 = r_0 \sqrt{\frac{1-a}{1-2a}} \tag{22}$$

where, α denotes the wind shear exponent; a is the axial induction factor; r_1 is the initial wake radius, and r_0 is the rotor radius. After the wake velocity distribution is obtained, the vertical wake deflection is determined. By assuming that θ in the wake region follows a top-hat distribution, the following expression is derived:

$$F_z \approx -\rho \int_{A_w} u_w^2 \theta \,\mathrm{dA} = -\theta\rho \int_{A_w} u_w^2 \,\mathrm{dA} \tag{23}$$

The integral term can be evaluated based on Eq. (19) as follows:

$$\int_{A_w} u_w^2 \,\mathrm{dA} \approx u_0^2 \pi \left(7.9\sigma_y\sigma_z - \frac{C_T^{'} D^2}{4}\right) \tag{24}$$

By substituting the evaluated integral into Eq. (23), the following expression is obtained:

$$\theta = -\frac{C_T D^2 \cos^2\varphi \sin\varphi}{63.2\sigma_y\sigma_z - 2C_T D^2 \cos^3\varphi} \tag{25}$$

By assuming $\theta \approx \tan\theta$, the following expression is obtained:

$$\theta \approx \frac{\mathrm{d}\delta_z}{\mathrm{d}x} \tag{26}$$

By letting $\frac{1}{k}\mathrm{d}\left(\sigma / D\right)$ replace $\mathrm{d}x$, and defining

$k=\sqrt{k_y k_z}, \sigma=\sqrt{\sigma_y \sigma_z}$, the following expression is obtained:

$$\frac{\delta_z}{D}=\frac{\sin\varphi\sqrt{C_T\cos\varphi}}{22.49k}\ln\left|\frac{\left(\sigma/D-0.178\sqrt{C_T\cos^3\varphi}\right)\left(\sigma_0/D+0.178\sqrt{C_T\cos^3\varphi}\right)}{\left(\sigma_0/D-0.178\sqrt{C_T\cos^3\varphi}\right)\left(\sigma/D+0.178\sqrt{C_T\cos^3\varphi}\right)}\right|+\frac{\delta_{z0}}{D} \tag{27}$$

The subscript 0 denotes the value evaluated at the downstream location where the wake profile becomes self-similar. Following Bastankhah and Porté-Agel (2016), the skew angle at the rotor plane, θ_r , is computed as follows:

$$\theta_r=\frac{0.3\varphi}{\cos\varphi}\left(1-\sqrt{1-C_T\cos\varphi}\right) \tag{28}$$

Considering that wake expansion in the near-wake region can lead to a slight increase in θ , the skew angle is assumed to be $\theta_0=k\theta_r$, where the coefficient k is set to 1.3. By equating Eq. (28) with Eq. (25), the following solution is obtained:

$$\frac{\sigma_0}{D}=\sqrt{\frac{C_T\cos^2\varphi\left(\sin\varphi+2\theta_0\cos\varphi\right)}{63.2\theta_0}} \tag{29}$$

By substituting x_0 back into the expression for the standard deviation, the corresponding parameter can be obtained. It should be noted that x_0 is not intended to precisely determine the onset location of wake self-similarity; instead, it is introduced to provide parameters for the analytical wake model. The main expressions of the proposed analytical wake model are given by Eq. (20) and Eq. (27).

Model Validation

The time-averaged flow field data obtained from LES are used as the reference for validation of the proposed model. Case 2 and Case 3 are selected for validation, and comparisons are also conducted against existing analytical wake models (Bastankhah and Porté-Agel, 2014; He et al., 2021). Fig. 13 compares the predicted vertical wake deflection with the LES results. It is shown that the proposed model captures the vertical wake deflection induced by the platform pitch offset, and good agreement is observed with the LES results.

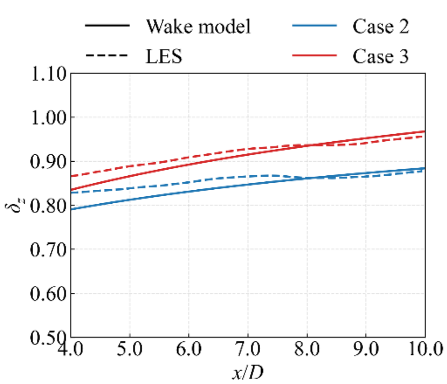

Fig. 13. Comparison of the vertical wake deflection

Figs. 14 and 15 present comparisons of the velocity deficit profiles at several downstream locations for Case 2 and Case 3, respectively. Overall, on the horizontal plane, the proposed model achieves higher accuracy than the reference models. On the vertical plane, the proposed model provides a more reasonable representation of the overall vertical wake deflection.

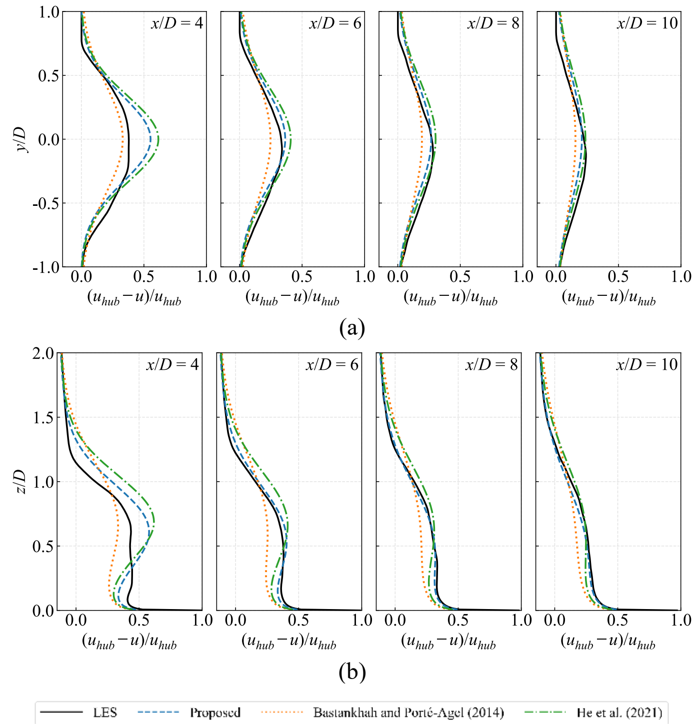

Fig. 14. Comparisons of normalized velocity deficit profiles for Case2: (a) horizontal plane; (b) vertical plane

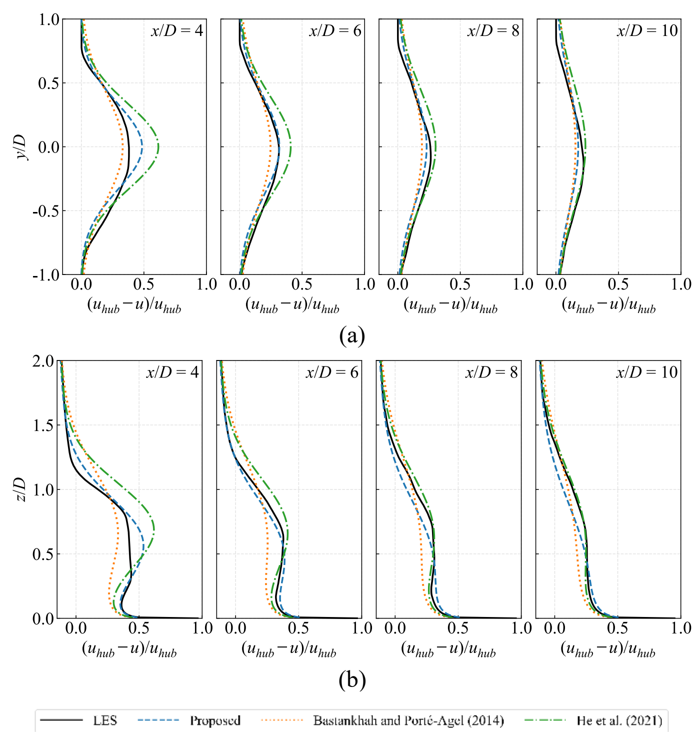

Fig. 15. Comparisons of normalized velocity deficit profiles for Case3: (a) horizontal plane; (b) vertical plane

Table 2 and Table 3 summarize the normalized root mean square error (NRMSE) values of different analytical wake models for Case 2 and Case 3 on the horizontal and vertical planes, respectively. Quantitatively, the proposed model shows higher overall accuracy than the other models. However, at 8*D* and 10*D* downstream in Case 3, slightly lower NRMSE values are obtained by the model that does not explicitly account for vertical wake deflection. This behavior is likely due to the fact that the velocity deficit gradually approaches a self-similar distribution in the far wake, while the wake width expands with downstream distance, which reduces the influence of vertical wake deflection on the velocity profiles. Nevertheless, considering the overall statistical performance and the capability of predicting vertical wake deflection, the proposed model remains advantageous.

Table 2. NRMSE of the normalized velocity deficit profiles on the horizontal plane

Case	Wake model	4*D*	6*D*	8*D*	10*D*	Avg.
2	He et al.	0.284	0.144	0.137	0.158	0.180
	Bastankhah and Porté-Agel	0.143	0.164	0.190	0.216	0.178
	Proposed	0.207	0.097	0.116	0.150	0.143
3	He et al.	0.286	0.183	0.153	0.163	0.196
	Bastankhah and Porté-Agel	0.125	0.134	0.160	0.187	0.152
	Proposed	0.134	0.081	0.111	0.150	0.119

Table 3. NRMSE of the normalized velocity deficit profiles on the vertical plane

Case	Wake model	4*D*	6*D*	8*D*	10*D*	Avg.
2	He et al.	0.126	0.069	0.049	0.040	0.071
	Bastankhah and Porté-Agel	0.098	0.080	0.070	0.062	0.078
	Proposed	0.084	0.034	0.029	0.031	0.045
3	He et al.	0.122	0.057	0.037	0.031	0.063
	Bastankhah and Porté-Agel	0.091	0.075	0.063	0.055	0.071
	Proposed	0.052	0.035	0.044	0.047	0.044

CONCLUSIONS

Numerical simulations are conducted in this study using the LES-ALM approach to model an FOWT under ABL inflow conditions with a platform pitch offset. The influence of pitch on wake structures is examined, and a new analytical wake model is developed accordingly. The main conclusions are summarized as follows:

(1) The numerical results indicate that, on the vertical plane through the rotor center, the wake centerline exhibits a clear overall upward shift with increasing platform pitch offset.

(2) The velocity deficit profiles of both the FOWT and FBWT exhibit an approximately double-peaked shape in the near wake and gradually transition to a single-peaked Gaussian-like distribution with downstream distance. Gaussian fitting results show good agreement with a Gaussian distribution in the far wake.

(3) Based on the analysis of the LES results, an analytical wake model applicable to FOWTs is proposed. The model is derived from momentum conservation and assumes a two-dimensional Gaussian form for the wake velocity distribution. Following the modeling strategy of yawed-wake formulations, a vertical component of the rotor-induced force associated with an effective inclination angle is introduced, leading to an expression for vertical wake deflection, and a wind-shear correction is further incorporated.

(4) Validation against LES results demonstrates that the proposed model captures the vertical wake deflection induced by the platform pitch offset and provides accurate predictions of the far-wake velocity deficit profiles at multiple downstream locations.

Future work can be directed toward further improving the model, including enhancing the prediction of wake width and extending the applicability and accuracy under a wider range of operating conditions.

ACKNOWLEDGEMENTS

This work was supported by the National Key Research and Development Program of China (2025YFF0519800), to which the authors are most grateful.

REFERENCES

Bastankhah, M, and Porté-Agel, F (2014). “A new analytical model for wind-turbine wakes,” *Renewable Energy*, 70, 116–123.

Bastankhah, M, and Porté-Agel, F (2016). “Experimental and theoretical study of wind turbine wakes in yawed conditions,” *J Fluid Mech*, 806, 506–541.

Bhattacharya, S, and Nikitas, G (2025). “Wind energy: status and outlook with focus on offshore wind,” *Energy and Climate Change*, Elsevier, 197–224.

Cai, Y, Li, X, Leng, S, Zhao, H, and Zhou, Y (2024). “Effect of combined surge and pitch motion on the aerodynamic performance of floating offshore wind turbine,” *Ocean Engineering*, 306, 118061.

Churchfield, MJ, Lee, S, Michalakes, J, and Moriarty, PJ (2012). “A numerical study of the effects of atmospheric and wake turbulence on wind turbine dynamics,” *Journal of Turbulence*, 13, N14.

Fan, S, and Liu, Z (2025). “Wind tunnel investigation of wake dynamics of floating offshore wind turbines under different inflow conditions and pitch-surge coupling,” *Renewable Energy*, 248, 123155.

He, R, Yang, H, Sun, H, and Gao, X (2021). “A novel three-dimensional wake model based on anisotropic Gaussian distribution for wind turbine wakes,” *Applied Energy*, 296, 117059.

He, R, Deng, X, Li, Y, Dong, Z, Gao, X, Lu, L, Zhou, Y, Wu, J, and Yang, H (2023). “Three-dimensional yaw wake model development with validations from wind tunnel experiments,” *Energy*, 282, 128402.

Jensen, NO (1983). *Risø-M. 2411: a note on wind generator interaction*.

Jonkman, J, Butterfield, S, Musial, W, and Scott, G (2009). “Definition of a 5-MW Reference Wind Turbine for Offshore System Development.,”

Li, W, Zhao, Z, Liu, Y, Liu, H, Wei, S, Ali, K, Dong, G, Liu, Y, and Ma, Y (2025). “Investigation of dynamic wake model of a floating offshore wind turbine under heave, surge and pitch motion,” *Renewable Energy*, 254, 123665.

Li, Y, Yu, W, and Sarlak, H (2024). “Wake Structures and Performance of Wind Turbine Rotor With Harmonic Surging Motions Under Laminar and Turbulent Inflows,” *Wind Energy*, 27(12), 1499–1525.

Liu, M, Zhong, Y, Zhao, W, and Wan, D (2025). “Effect of coupled surge–pitch motions on the wake characteristics of floating offshore wind turbines under atmospheric boundary layer inflows," *Physics of Fluids*, 37(11), 115115.

Messmer, T, Peinke, J, Croce, A, and Hölling, M (2025). "The role of motion-excited coherent structures in improved wake recovery of a floating wind turbine," *J Fluid Mech*, 1018, A23.

Moeng, C-H (1984). "A Large-Eddy-Simulation Model for the Study of Planetary Boundary-Layer Turbulence," *J Atmos Sci*, 41(13), 2052–2062.

Smagorinsky, J (1963). "General circulation experiments with the primitive equations: i. the basic experiment," *Mon Wea Rev*, 91(3), 99–164.

Sørensen, JN, and Shen, WZ (2002). "Numerical Modeling of Wind Turbine Wakes," *Journal of Fluids Engineering*, 124(2), 393–399.

Wang, L, Dong, M, Yang, J, Wang, L, Chen, S, Duić, N, Joo, YH, and Song, D (2024). "Wind turbine wakes modeling and applications: Past, present, and future," *Ocean Engineering*, 309, 118508.

Wei, D-Z, Wang, N-N, and Wan, D-C (2021). "Modelling Yawed Wind Turbine Wakes: Extension of a Gaussian-Based Wake Model," *Energies*, 14(15), 4494.

Xu, S, Zhuang, T, Zhao, W, and Wan, D (2023). "Numerical investigation of aerodynamic responses and wake characteristics of a floating offshore wind turbine under atmospheric boundary layer inflows," *Ocean Engineering*, 279, 114527.

Zhang, H, Gao, X, Lu, H, Zhao, Q, Zhu, X, Wang, Y, and Zhao, F (2024a). "Investigation of a new 3D wake model of offshore floating wind turbines subjected to the coupling effects of wind and wave," *Applied Energy*, 365, 123189.

Zhang, P, Li, C, Wei, Y, and Wu, W (2024b). "Three-dimensional analytical wake model for floating offshore wind turbines under pitch motion," *Ocean Engineering*, 311, 118935.